



JOURNAL OF
APPLIED
CRYSTALLOGRAPHY

Volume 53 (2020)

Supporting information for article:

Complex modelling for the quantification of nanoscale disorder using genetic algorithms, density functional theory, and line profile analysis

Robert J. Koch, Guangfang Li, Shubham Pandey, Simon R. Phillpot, Hui Wang and Scott T. Misture

Differential evolution fitting was all done using the DIFFEV module of the DISCUS software package. During this process, each population member of a given generation was represented by supercell, with structural details governed by its parameter set. Chemical correlation coefficients $c_{\langle 100 \rangle}$ and $c_{\langle 110 \rangle}$ as defined by Welberry (Welberry, 1985) were refined as part of the optimization. The process to target a given pair of correlation coefficients for any supercell is outlined extensively in the book of Neder and Proffen (Neder & Proffen, 2008), specifically Section 5.3. The process is based on a Monte Carlo energy minimization of an Ising-type energy function of the form

$$E = \sum_i H\sigma_i + \sum_i \sum_{n \neq i} J_n \sigma_i \sigma_{i-n}$$

where sums are over all sites i and neighbor types n . The values σ_{i-n} and σ_i refer to the occupancy “spin” of the site i and its neighbor $i - n$ and can take on values of ± 1 . The strength of the occupancy spin interaction is controlled by the pair interaction energy J_n , while H is an energy term controlling the overall concentration. In this work, the interaction energies H and J_n were tuned during a feedback loop to target the nominal values of $c_{\langle 100 \rangle}$ and $c_{\langle 110 \rangle}$. This loop updated the energy terms every $50N$ iterations and ran for $500N$ iterations total, where N is the total number of atoms in the supercell. Several example configurations achieved through this process, associated with different permutations of $c_{\langle 100 \rangle}$ and $c_{\langle 110 \rangle}$ are shown in Fig. S4. Examples of the coordination environment histograms (see e.g. Fig. 8) resulting from these example configurations are shown in Fig. S5.

In Fig. S6 the optimization progress is shown for fit 4. The mean parameter values and standard deviations, as well as the logarithm of R_w , are all plotted as a function of the iteration number. In early iterations, the population standard deviations are large as the parameter space is explored to find many candidate solutions. The best of these survive, the parameters stop varying significantly during intermediate generations, and the objective function improvement becomes small, leading to satisfaction of the first convergence criterion. In the final generations, population members furthest from the mean are removed, and the population standard deviations decrease, leading to satisfaction of the second convergence criterion.

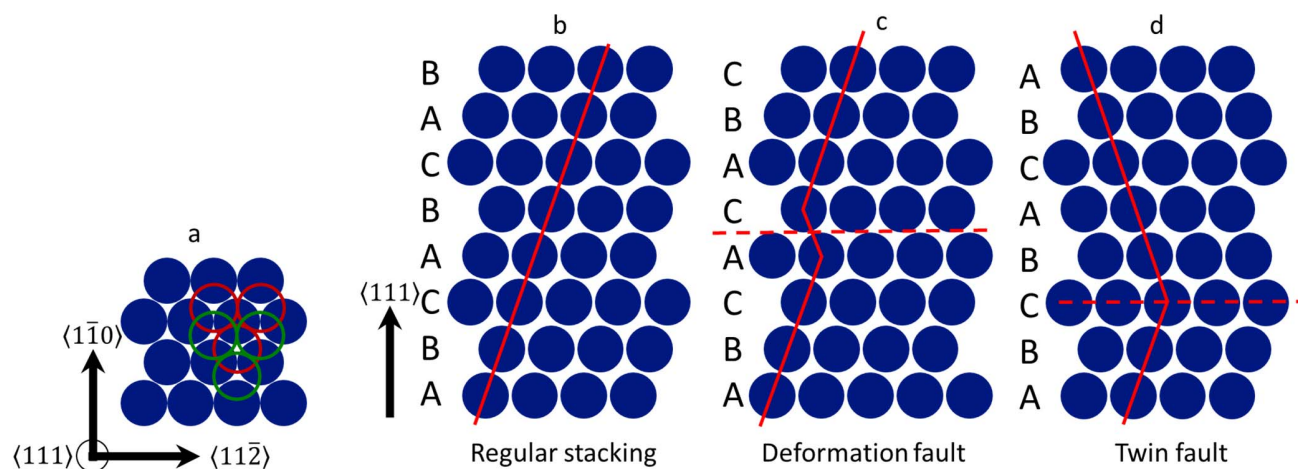


Figure S1 Diagram depicting the types of stacking faults in an FCC system. In (a) a projection down the $\langle 111 \rangle$ direction is shown, highlighting the three positions for a single layer of atoms (represented by closed blue or open green/red circles). Regular stacking, shown in (b), is often represented as an “...ABCABC...” sequence, where every third layer along the $\langle 111 \rangle$ direction has an identical horizontal position. A deformation fault, shown in (c), is represented as an “...ABCACABC...” sequence, and a twin fault, shown in (d), is represented as an “...ABCBACBA...” sequence. Fault locations are represented by dashed red lines.

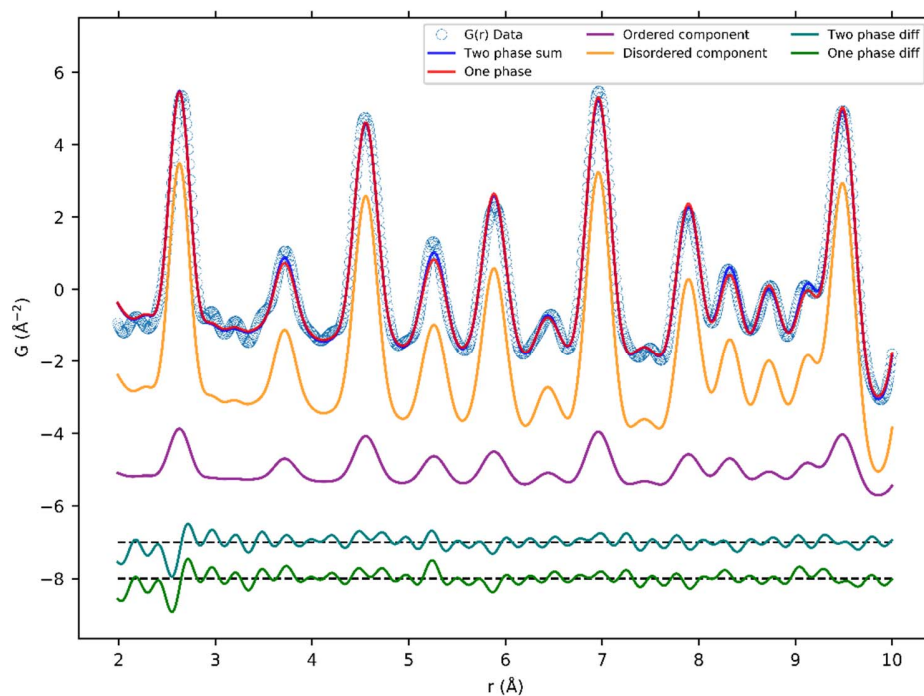


Figure S2 An example PDF fit over 2-10 Å using either a single disordered phase model, or a two phase model containing an ordered and disordered component. The two-phase fit corresponds to the lowest- r point in Figure 6. The components of the two phases contributing to the two-phase signal are also shown, with each fit residual, all offset vertically for clarity. Although the differences may seem small, they are on the same order as those observed by others (Proffen, 2000).

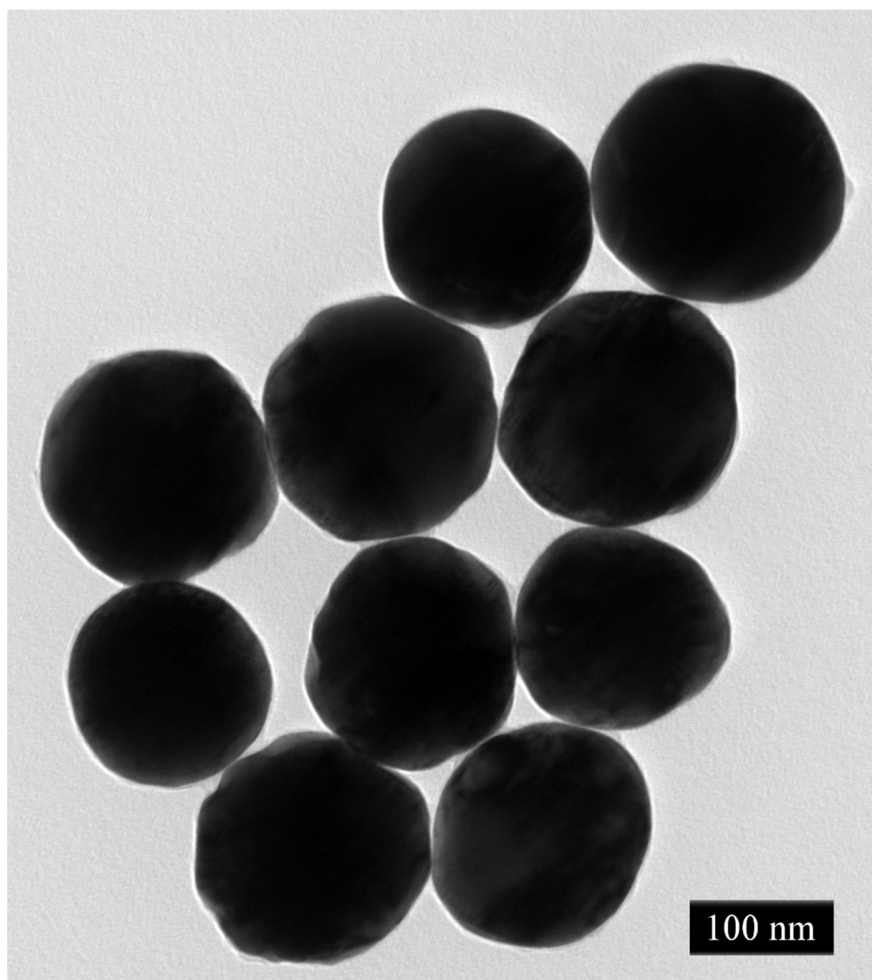


Figure S3 Transmission electron micrographs of the alloys studied in this work, obtained at an accelerating voltage of 200 kV.

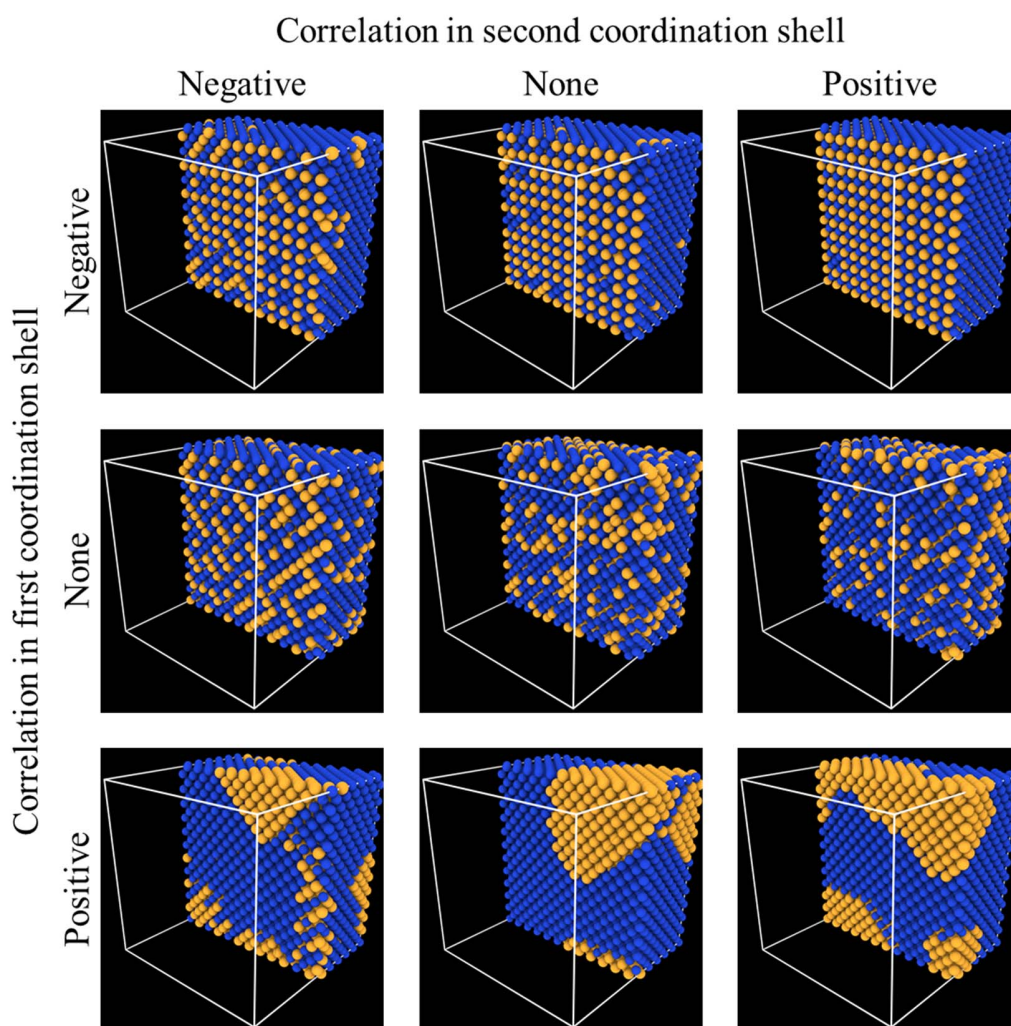


Figure S4 Example configurations for the 9 different ways of permuting positive, negative and zero values for the two different correlation parameters: $c_{\langle 110 \rangle}$, representing chemical correlation in the first CS, and $c_{\langle 100 \rangle}$, representing chemical correlation in the second CS.

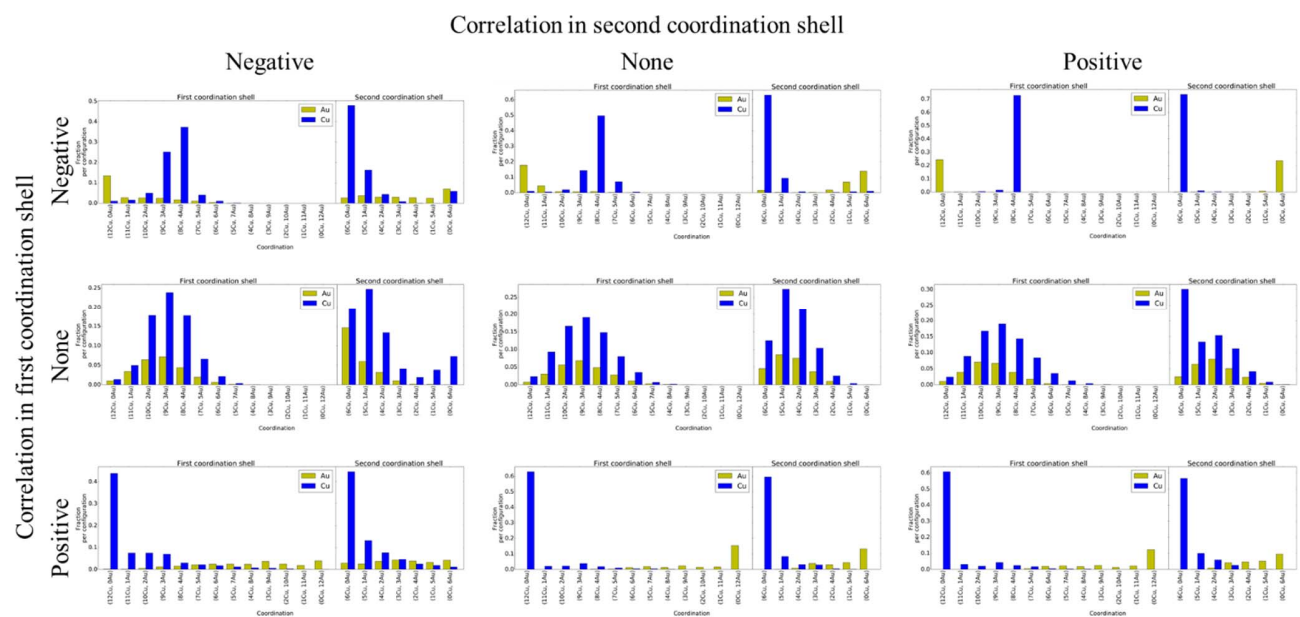


Figure S5 Histograms representing the average fraction of first and second CSs for the corresponding example configurations in Fig. S4.

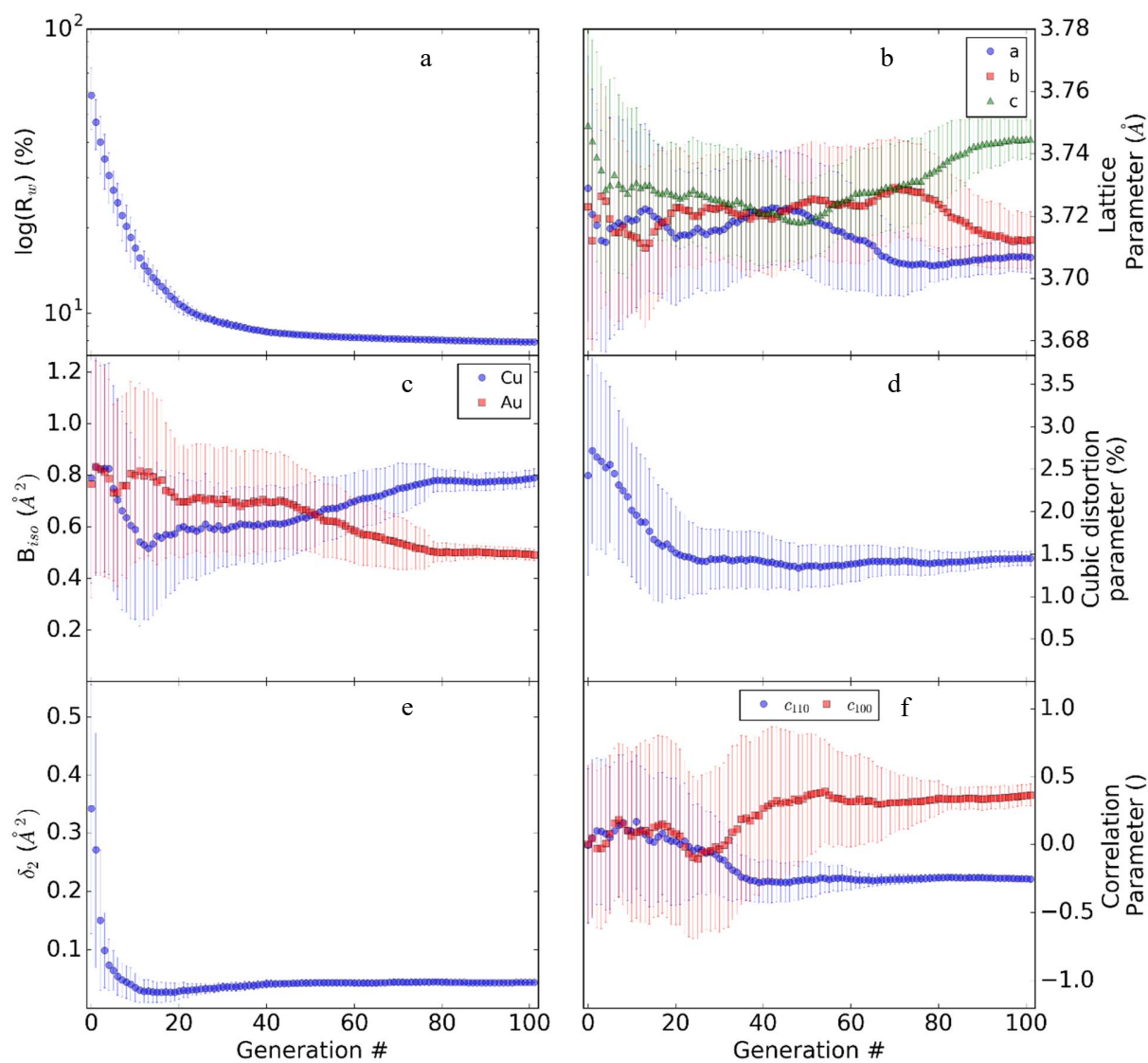


Figure S6 A plot of the optimization progress as a function of the iteration of generation number. In (a) the natural log of the fit quality index is plotted, in (b), the lattice parameters, (c) the isotropic thermal parameters, (d) the cubic distortion parameter, derived from the lattice parameters (see text for details), (e) the correlated thermal motion parameter, and (f) the chemical correlation motion parameters. The plotted points represent the population mean, while the error bars represent the population standard deviation.